PAPER

Check for updates

Sub-100 nm nanoplastics: potent carriers of tributyltin in marine water†

Jason Raymond, [ID] Monica Felipe-Sotelo, Rachida Bance-Soualhi, [ID] Carol Crean [ID] and Maya Al-Sid-Cheikh [ID]*

Despite laws prohibiting its usage, butyltin (TBT) is a legacy pollutant and an antifouling agent that is still prevalent in marine systems and has been shown to have negative effects on the ecosystem. The purpose of this study is to fill a vacuum in the literature by determining whether nanoplastics (NPs, <1000 nm) can carry TBT, which might provide a new TBT exposure pathway to marine organisms. Adsorption capacity was modelled using nanopolystyrene (PS-NP) with three particle sizes spanning the nano-range (40, 485 and 765 nm). Kinetics and thermodynamics of TBT adsorption by PS-NP were explored within natural sea water (32 psu), brackish water (16 psu), artificial sea water (32 psu), and a sodium monophosphate/diphosphate buffer (pH 8, 0.1 M). Elemental analysis, following adsorption experiments, was completed by inductively coupled plasma-mass spectrometry and microwave plasma-atomic emission spectroscopy. Between 78 and 99% of the total TBT adsorption occurred within the first 0–6 hours of mixing. Freundlich isotherm models provided the most accurate fit to experimental data for each water and polystyrene particle matrix (R^2 values between 0.9086 and 0.9970), suggesting that the system underwent non-ideal or multilayer adsorption. The greatest capacity for adsorption was observed with the smallest plastic particles (49.5–85.6% (m/m)) and within the brackish water matrix (40.0–85.6% (m/m)). This suggests that the adsorption capacity increases with decreasing particle size and salinity, highlighting that nanoplastics have greater potential to act as a vector for the transportation of TBT over microplastics, and that adsorption is restricted by the presence of competitive salts. Distribution coefficients (K_D) for TBT adsorption by PS-NP (between 193 ± 9 L g^{-1} and 2853 ± 291 L g^{-1}) are consistent with the upper range of literature reported values for sediment adsorption. This suggests that PS-NPs have similar potential for TBT adsorption to naturally occurring sediment particles. When considering the differences in specific gravity between NP and sediment particles, this research highlights a concern of increased TBT mobility when bound to NPs, and the potential for TBT to become more available to surface-dwelling organisms such as those residing in tidal zones.

Environmental significance

The behaviour of nanoplastics (NPs) and their subsequent interactions with environmental co-contaminants are not fully understood. The types of co-contaminants and environmental matrices are crucial in estimating their bioaccumulation and bioavailability to organisms, allowing us to predict their potential impact. Here, we quantify the adsorption capacity of tributyltin (TBT), a former antifoulant remaining in the environment, by nanopolystyrene in brackish water, artificial and natural seawater, at environmentally realistic concentrations of NP and TBT. This helps to determine whether: i) TBT can be remobilised by NPs, ii) there is a synergistic effect once adsorbed onto the particles, and iii) TBT is bioavailable once ingested.

Introduction

Over the last 60 years, plastic's accumulation on the Earth has become one of the most prominent human impacts on the environment. 8.3 billion tonnes of plastic have been produced since 1950, with an estimated 7.3 billion tonnes still existing in some form today.[1] Larger plastic debris in the ocean undergoes degradation into smaller particles, from macro- to microplastics (MPs, <5 mm).[2] It is predicted that between 93 and 236 thousand tonnes of MPs have contaminated the world's oceans.[3] MPs have been shown to be utterly ubiquitous; their presence found in seafood,[4–6] cow and breast milk,[7,8] airborne dust,[9] bottled water[10–12] and plastic teabags.[13] Studies show that bivalves sold in Chinese fishery markets can contain 2.1 to 10.5 particles of

School of Chemistry and Chemical Engineering, University of Surrey, Stag Hill, Guildford, GU2 7XH, UK. E-mail: m.alsidcheikh@surrey.ac.uk

† Electronic supplementary information (ESI) available. See DOI: https://doi.org/10.1039/d3en00659j

This journal is © The Royal Society of Chemistry 2024

Environ. Sci.: Nano, 2024, **11**, 241–252 | **241**

plastic per gram.[14] There is now evidence suggesting that further fragmentation occurs, from MPs to nanoplastics (NPs, <1000 nm).[15] Recently, it has been highlighted that NPs are the least investigated in the literature, despite them potentially being the most hazardous.[15,16] NPs are expected to be even more widespread and accumulate in seafood.[5] Determining the behaviour of MP and NP particles in the ocean is crucial to assess the risk they exert in the environment, as well as the multiple human exposure routes that these particles have.

The capacity of plastic particles to adsorb other toxic compounds (TCs) present in the environment has become a cause for concern within the MP debate. Adsorption of TCs onto the plastic's surface, if occurring, would enable the plastic particles to vectorise these compounds. Most of the current studies looking at the adsorption capacity of TCs by plastic particles focus exclusively on MPs.[17] Previous research has shown that MPs sorb hydrophobic organic contaminants.[18-20] It is also apparent that sorption behaviour between MPs and organic TCs is complex and unclear, due to the number of mechanisms by which it can occur.[18,21] For example, MPs can undergo pore filling, hydrophobic partitioning, hydrogen bonding, van der Waals, electrostatic and π–π interactions.[22,23] The adsorption of TCs is dependent on several factors such as the shape, composition, and age of plastic particles, as well as the type of adsorption mechanism and environmental conditions such as pH, concentration, and temperature. In the literature, there is conflicting evidence for the impact of polymer type, with research suggesting that the polymer type both does[24,25] and does not[26] have a substantial impact on the adsorption capacity. It is common for MP research to conduct adsorption experiments with polystyrene particles,[27] likely due to their absence from blanks and commercial availability. The size of the plastic particles is shown to have a significant effect on their adsorption properties,[28] as an increased surface to volume ratio leads to a greater number of available binding sites. NPs have a larger surface area when compared to MPs and it is thereby expected that NPs exhibit greater adsorption capacity than MPs. Very few literature studies report values for adsorption onto NPs, with maximum adsorption capacity examples of 8710 $\mu g\ g^{-1}$ by 40 nm PS particles with bisphenol A and ciprofloxacin and 970 000 $\mu g\ g^{-1}$ by 150–450 nm PS particles with Pb.[29] The distribution coefficient (K_D) for polychlorinated biphenyls by 361 nm PS was determined as 10^4 to 10^9 L kg^{-1}.[30]

Tributyltin (TBT) was used extensively in the early 1970s as an antifouling agent on the underside of marine vessels. The toxicity of TBT has therefore received large amounts of interest in the literature due to the global effects on marine organisms by the poisoning of barnacles, algae, and other organisms at the bottom of the food chain.[31] One of the most frequently cited impacts of TBT pollution is the induced imposex within the mollusc population, a condition characterised by the super-imposition of male genitalia onto female gastropods. The exact cause of imposex induction is a

subject of ongoing research, however it is theorised to follow one of three mechanisms: abnormal release of the neuropeptide APGWamide,[32] elevated testosterone levels[33,34] or the displacement of the natural 9-*cis* retinoic acid by organotins from the retinoid X receptor (RXR).[35] Population decline of several species has been attributed to organotin derived imposex, and widespread imposex continues to be reported.[36,37] This highlights that although TBT is considered a legacy pollutant, its persistence in marine systems and its ongoing environmental impacts require continued research and monitoring.[38] In addition, TBT itself has been shown to affect the growth and mortality of molluscs and bivalves.[39-42] Larvae and developing bivalves are especially sensitive to TBT exposure.[41] Toxic effects in some species occur for lower than 1 ng TBT per litre of water.[31] Accumulation of TBT within marine organisms has highlighted concerns for human exposure, with predicted daily intakes by humans estimated at 0.25 μg per kg of body weight, per day.[34] Despite regulation introduced in the 1980s (UK: 1987, France: 1982 and US: 1988 (ref. 43)) which prevented its use, TBT continues to be used on military vessels and in some developing countries with less strict regulations.[44] TBT-containing biocide products are also still manufactured and commercially available.[45] The high hydrophobicity of TBT results in strong affinity to suspended marine particles such as sediments and plastics.[46,47] When bound to these suspended particles, TBT has a significantly longer half-life (up to 40 years). TBT has been shown to have an especially strong affinity towards plastic surfaces, where it has been shown to be removed from the aqueous phase *via* adsorption.[48] Although TBT has a high specific gravity and predominantly exists within the benthic region of the ocean, NPs and MPs are significantly less dense,[49] so TBT adsorption onto these particles may cause its remobilisation, potentially leading to further TBT-caused environmental fallout.

This research aims to fill the current research gap by providing understanding of the impact of salinity and particle size across both environmental and elevated concentrations. This will be achieved by completing the following objectives: (1) to produce and characterise nanopolystyrene particles (PS-NP) in varying sizes across the nano-range (between 1 μm and 1 nm); (2) conduct adsorption experiments, using varying salinity, adsorbate concentration and adsorbent particle size; (3) determine the most appropriate adsorption isotherm for modelling adsorption behaviour, and subsequently calculate adsorption capacities and distribution coefficients for each matrix.

Methodology

Nanopolystyrene particle synthesis

Nanopolystyrene (PS-NP) was prepared and purified according to Al-Sid-Cheikh *et al.*, 2020.[50] Three distinct sizes of PS-NP were produced: 40 nm (small, 39.5–41.2 nm diameter), 480 nm (medium, 476–495 nm diameter) and 760 nm (large, 727–823 nm diameter). The concentration of the

final purified particles was determined by direct weighing of an aliquot of the reaction suspension, before and after removal of the solvent by freeze-drying. Concentrations for small, medium, and large PS-NPs were found to be 120 400 ± 8990 μg mL^{-1}, 65 960 ± 9454 μg mL^{-1} and 56 360 ± 11 292 μg mL^{-1} respectively. These were also converted to concentration in the form of particle number per volume,[51] giving 3.40 × 10^{15} ± 2.54 × 10^{14} particles per mL, 1.06 × 10^{12} ± 1.52 × 10^{11} particles per mL and 2.29 × 10^{11} ± 4.58 × 10^{10} particles per mL for small, medium and large PS-NPs respectively.

Characterisation by dynamic light scattering (DLS), Brunauer, Emmett and Teller (BET) surface area analysis, thermogravimetric analysis (TGA), Fourier-transformed infrared spectroscopy (FTIR), Raman and scanning electron microscopy (SEM) was completed to determine the physical and chemical properties of the produced particles. Samples for DLS (Zetasizer Nano-S, Malvern Panalytical, UK) were prepared in disposable cuvettes at 2.0 μg mL^{-1} in Milli-Q water (18.2 MΩ), sonicated, and allowed to equilibrate for 120 seconds and then replicate analysis (10 measurements and 10 replicates) was completed at room temperature. BET analysis, TGA, Raman and FTIR all require, or benefitted from, dry (or semi-dry) samples; therefore, an aliquot of each PS-NP was freeze-dried under reduced vacuum to complete the characterisation. For FTIR (Spectrum 2, Perkin Elmer, UK), samples were placed directly onto an attenuated total reflection (ATR) crystal for analysis. For Raman (InVia Reflex Raman Microscope, Renishaw, UK), dry PS-NP powders were placed on a stage and scanned using 785 nm laser excitation (near-IR line laser, 100% laser power) and a 50XL objective. Dry samples for TGA (Q500, TA Instruments, US) were placed directly onto a platinum sample pan under a nitrogen atmosphere. Data were obtained between 20 °C and 600 °C at a ramp rate of 10 °C min^{-1}.

In preparation for BET surface area analysis, a gentle disaggregation of the freeze-dried PS-NP powders (~0.5 g) was performed by milling in falcon tubes (150 rpm, 5 minutes, Retsch MM440, Germany) with stainless steel balls (VWR Grinding Balls, 10 mm), to break apart groups of particles. No changes in particle structure were observed by SEM. The disaggregated powders were then placed in a vacuum desiccator (72 h) to perform a preliminary outgassing at room temperature. BET tubes were loaded with ~0.2 g of outgassed PS powder and a further outgassing was performed in the Quantachrome™ NOVA chamber (72 h, 70 °C). This process was optimised to be as gentle as possible, without subjecting the PS-NP particles to temperatures close to the polystyrene glass transition temperature (99 °C).[52] Once outgassed, adsorption and desorption curves were obtained under nitrogen between relative pressures (P/P_O) of 0.1 and 0.99.

For SEM (Apreo 2, Thermo Fisher Scientific, UK and JSM-7100F, JEOL, Japan) sample preparation, 20 μL aqueous PS-NP suspension was placed directly on an aluminium stub, allowed to settle for 15 minutes, and dried via capillary action using filter paper, before a 6 nm gold coat was applied. Analysis was completed using an Everhart–Thornley detector (ETD) set within 0.02 to 0.2 nA and 2 to 20 keV, however this was optimised when required to obtain images with the desired focus and magnification images.

Kinetics of TBT adsorption onto PS-NP

Adsorption as a function of time was measured to determine the time taken to reach equilibrium within the TBT/PS-NP system. Tri-n-butyltin chloride (TBT, 95% tech., Thermo Scientific Acros, UK) standards (100 ng mL^{-1} TBT, representative of TBT concentrations within environmental sediments,[34] whilst remaining above the instrument detection limit) were prepared in a pH 8 buffer (0.1 mol dm^{-3}, di- and mono-basic sodium phosphate buffer in Milli-Q water), natural seawater (NSW) taken from Havant Bay, Portsmouth (50.834376, −1.036339) and artificial seawater (ASW). pH 8 was chosen for the buffer solution to mimic the environmentally occurring pH in open ocean,[53] and NSW and ASW were measured at pH 8.1. ASW was prepared via dilution of artificial sea salt (Ocean Reef Pro Coral Salt, iQuatics, UK) in Milli-Q water (up to a salinity of 32 psu). Scoping experiments were conducted to compare spike recoveries of TBT from plastic (polypropylene, Sarstedt, Germany) and glass (low potassium borosilicate glass, Dixon Science, UK) sample vessels (the average TBT recovery in plastic and glass vessels was found to be 29.2 ± 4.0% and 79.9 ± 4.5% respectively). Therefore, subsequent adsorption experiments were conducted in glass (scintillation vials, 20 mL, V0044, Dixon Science, UK) to reduce the loss of TBT to the walls of the sample vessel. The solutions were spiked with the appropriate volume of PS-NP to give a concentration of 2.0 μg mL^{-1} PS (small PS: 5.65 × 10^{10} particles per mL, medium PS 3.21 × 10^7 particles per mL and large PS 8.11 × 10^6 particles per mL, chosen to facilitate measurement of K_D within the detection capabilities of the instrument) in each vial and added to an orbital mixer at 125 rpm (PSU-20i orbital mixer, Grant-bio, UK). Adsorption experiments were conducted at room temperature, monitored continually by a temperature probe (18.61–24.35 °C, IBS-TH2, Inkbird, China). Vials were removed from the mixer at increasing time intervals in order to measure the amount of TBT remaining in solution at each time (1 h, 3 h, 5 h, 12 h, 24 h and 48 h, each with 3 replicates). PS-NP solutions without the presence of TBT were agitated across the same time period to provide TBT blanks. The samples were filtered using a method appropriate to their size and the supernatant was acidified up to 4% (v/v) nitric acid (trace metal grade, Fisher Chemical, US). For the two larger particle sizes, it was possible to use micrometre syringe filters to separate the PS-NP phase (0.22 μm: Millex®-GP, Millipore Express® PES Membrane. 0.45 μm: Millex®HA, Millipore MCE Membrane, Merck, Ireland); however, for the smallest particles, an ultrafiltration method was optimised using filtration membranes (30 kDa, DiaFlo® YM30, Amicon Corporation, US) under a gentle nitrogen pressure. The loss of TBT to each of the filters was assessed during spike recovery experiments (Table S1 in the ESI†).

This journal is © The Royal Society of Chemistry 2024

Environ. Sci.: Nano, 2024, **11**, 241–252 | **243**

Thermodynamics of TBT adsorption

Once the time taken to reach equilibrium had been established, adsorption was measured across 24 hours within 4 water matrices: pH 8 buffer in Milli-Q water, NSW, intermediate artificial seawater (BW, salinity of 16 psu) and ASW. These water matrices were used as a diluent to produce 3 replicates each of TBT standards (10, 50, 75, 100, 125, 150, 200 ng mL^{-1} TBT) in scintillation vials (20 mL, V0044, Dixon Science, UK). The concentration range was limited by the instrument detection limit (between 0.48 and 1.27 ng mL^{-1}) after adsorption on the lower end, and by the TBT solubility limit on the upper end. However, the standard concentration range was also chosen based on environmentally occurring concentrations within marine sediments and open ocean.[34] To determine whether the upper limit of adsorption was truly limited by the solubility limit, additional data points at 0.1, 0.5, and 1.0 ng mL^{-1} TBT and 2, 5, 10 and 50 μg mL^{-1} TBT were prepared in the pH 8 phosphate buffer to view the point of saturation. Each size PS-NP was added up to 2.0 μg mL^{-1} PS into each vial and the vials were placed on an orbital mixer for 24 hours. The aliquots of the supernatants were filtered using a method appropriate to their size and the supernatant was acidified up to 4% (v/v) nitric acid (trace metal analysis, Fisher Scientific) and kept refrigerated until analysis.

Elemental analysis

Samples were diluted 1 in 10 prior to analysis with inductively coupled plasma-mass spectrometry (ICP-MS, 7800 Series, Agilent Technologies, UK); the high matrix option was also employed.[54] For ICP-MS analysis, matrix-matched calibration standards were prepared between 0.1 and 20.0 ng mL^{-1} TBT with 4% (v/v) nitric acid in each of the water matrices. Additionally, two QC (quality control) samples were prepared in each acidified matrix at 0.25 and 2.5 ng mL^{-1} TBT. A methodology for the quantification of total Sn was developed using the ^{120}Sn isotope (33% abundance) and ^{115}In as internal standards. The following plasma conditions (no collision gas) were used: nebuliser pressure: 289 kPa; IF/BK pressure: 290 kPa; analyser pressure: 6.75 × 10^{-5} Pa; RF power: 200 V; uptake time: 15 s; rinse time: 60 s; stabilisation time: 30 s; replicates: 3; sweeps per replicate: 100. The limit of detection (LOD), limit of quantification (LOQ) and limit of linearity (LOL) were found to be 0.48, 1.61 and 516 ng mL^{-1} TBT respectively in the pH 8 phosphate buffer; 0.90, 4.52, and 499 ng mL^{-1} TBT in ASW; and 1.27, 6.37 and 504 ng mL^{-1} TBT in NSW. The QC recovery ranged between 82 and 112% throughout the analysis.

For the analysis of samples over the LOL of the ICP-MS (*i.e.* >500 ng mL^{-1} TBT), microwave plasma-atomic emission spectroscopy (MP-AES, 4210 Series, Agilent Technologies, UK) was used for quantification of TBT. Calibration standards and QCs were prepared in the same manner as for ICP-MS, with concentrations between 0.1 and 50.0 μg mL^{-1} TBT for standards and 2.5 and 25.0 μg mL^{-1} TBT for the two QCs. A

methodology for the quantification of the total Sn was developed using the emission line at 283.999 nm, applying Be 234.861 nm emission as the internal standard. The analyte emission line was chosen for its emission intensity and freedom from interferences. The following plasma conditions were used: plasma temperature: 50 °C; nebuliser pressure: 247 kPa; nebuliser flow: 0.5–0.9 L min^{-1}; gas box supply voltage: 24.1 V; pump speed: 15–80 rpm; uptake time: 30 s; rinse time: 60 s; stabilisation time: 15 s; number of replicates: 3. The limit of detection (LOD), limit of quantification (LOQ) and limit of linearity (LOL) were found to be 0.4, 1.6 and 25.0 μg mL^{-1} TBT respectively in the pH 8 phosphate buffer. The QC recovery ranged between 79 and 131% throughout the analysis.

Isotherm modelling

Adsorption behaviour was modelled using the Freundlich isotherm (eqn (1)).

$$Q_e = K_F C_e^{1/n} \tag{1}$$

where Q_e is the adsorption capacity at equilibrium, K_F and n are Freundlich constants and C_e is the concentration at equilibrium.

The Freundlich constant (K_F) refers to a product of the adsorption affinity (K_A) and the maximum adsorption capacity (Q_{max}). n can be used as an indicator of the adsorption intensity; a lower n value is indicative of a favourable adsorption. The distribution coefficient (K_D, μg L^{-1}) demonstrates the extent of adsorption by each PS-NP in each matrix at equilibrium, in terms of concentration of TBT bound to the PS-NP (C_{bound}, μg g^{-1}) and concentration of TBT in the aqueous phase ($C_{aqueous}$, μg L^{-1}) (eqn (2)).

$$K_D = \frac{C_{bound}}{C_{aqueous}} \tag{2}$$

where K_D is the distribution coefficient (μg L^{-1}), C_{bound} is the concentration of adsorbate bound to the adsorbent and $C_{aqueous}$ concentration of adsorbate in the aqueous phase. This model provides an accurate representation of the maximum adsorption capacity at the point where the concentration of TBT is approaching saturation (the TBT concentration beyond which, the concentration of bound TBT remains constant, irrespective of increases in the aqueous TBT concentration). At the point of saturation, C_{bound} is equal to the adsorption capacity and $C_{aqueous}$ is equal to the saturation concentration. Therefore, in the present study, K_D for TBT adsorption by PS-NP within each matrix is calculated using the ratio between the maximum adsorption capacity and the saturation concentration.

Adsorption capacity was approximated as the amount of TBT bound to the surface of the plastic at the aqueous solubility limit of TBT (eqn (3)). Here, the aqueous concentration of TBT at the solubility limit of TBT is denoted as C_{sat}. At this point, the PS particles will have scavenged the

244 | *Environ. Sci.: Nano*, 2024, **11**, 241–252

This journal is © The Royal Society of Chemistry 2024

maximum amount of TBT from the aqueous phase (*i.e.* where $Q_e \approx Q_{max}$).

$$Q_{sat} = K_F(C_{sat} \text{ ng mL}^{-1})^{1/n} \tag{3}$$

where Q_{sat} is the adsorption capacity at the limit of TBT solubility, K_F and n are Freundlich constants and C_{sat} is the aqueous TBT concentration at the limit of TBT solubility.

The solubility of TBT is dependent on several factors, including the temperature, media, equilibration time, presence of other solutes, and amount of agitation. For this approximation, the solubility limit of TBT was taken from previous work by Inaba *et al.*, 1995.[55] Here, the solubility of TBT in artificial seawater at room temperature is given as 300 ng mL^{-1} TBT between pH 7 and 8. The experimental conditions used by Inaba *et al.* are closely matched to the conditions used during adsorption experiments within the present study and can therefore provide the upper limit for the adsorption isotherm.

Results and discussion

Characterisation of PS-NP

The size of the small, medium, and large PS-NPs was determined to be 40 (39.6 to 41.2 nm), 484 (476 to 495 nm) and 770 (727 to 823 nm) respectively by DLS. Instrument measured diameter ranges obtained during the 10 measurements are given in brackets. The particle size was then confirmed by visual analysis of SEM images. DLS size distribution curves are given in Fig. S1 in the ESI.† SEM images at 10 000× and 100 000× magnification of each particle size are given in Fig. S2–S4 in the ESI.†

Surface area analysis of the small, medium, and large PS-NPs approximated the surface areas as 109 ± 5, 2.3 ± 0.1 and 1.2 ± 0.1 m^2 g^{-1} respectively. BET adsorption isotherms for each particle size are given in Fig. S5–S7 in the ESI.† The BET adsorption isotherms for each particle size (less prominent with small PS-NP) show a distinctive stepped pattern, suggesting the formation of multiple adsorption layers on a uniform, non-porous surface.[56] The sharpness of the stepwise shape is dictated by the adsorbent, adsorbate, and temperature.[57]

The purity of PS-NPs was determined using TGA. TGA mass and derivatised plots are given in Fig. S8 in the ESI.† It was found that the large and medium particles underwent degradation as single fractions, resulting in a sharp peak at 396 °C for both particles. This indicates that the large and medium PS-NP particles were close to 100% purity. The small PS-NP degraded into 3 fractions, at 161, 185 and 375 °C. The latter is consistent with the initial decomposition temperature (IDT) for PS particles,[58,59] accounting for a purity of 84.4%. The fractions at 161 and 185 °C accounted for 8.8% and 6.8% respectively. The impure fraction at 185 °C corresponds to the residual surfactant (sodium dodecyl sulphate, IDT: 180 °C (ref. 60 and 61)) from the synthesis. The fraction at 161 °C may correspond to the residual

initiator (potassium persulphate), although there are no current literature values to support this. It is undetermined whether the presence of these impurities influence the adsorption properties of the small PS-NP particle. SDS is a large organic molecule, which may cause some steric hindrances on the surface of the particle, restricting adsorption. Therefore, further work should investigate the implications of such impurities.

Raman and FTIR analysis of each PS-NP size were compared with that of the monomer, styrene, to confirm that complete polymerisation had occurred, and that polystyrene had been produced. In FTIR, the C–H alkane absorbance is not present in styrene, so this was the key factor when distinguishing between the polymer and monomer. Overlayed Raman spectra are given in Fig. S9 in the ESI,† and overlayed FTIR spectra are given in Fig. S10 in the ESI.†

Kinetics of TBT adsorption onto PS-NP

Kinetics experiments (Fig. 1) for each particle size in Milli-Q water, NSW and ASW were used to determine the optimum time for complete adsorption of TBT for each of the 3 sizes of PS-NP. It was found that adsorption by both large and medium PS-NP equilibrated after 3 hours, whilst the small PS particles had equilibrated after 12 hours (Student's one-tail *t*-test, $p = 0.05$). The slower equilibration time by the smallest PS-NP may be explained by the greater number of binding sites to fill, or due to the impurities observed in TBT, which are only present in the smallest particles. The results suggest that adsorption of TBT by PS-NP is slower than that by sediments, as Langston and Pope, 1995 (ref. 47) found that the majority of TBT adsorption by sediments occurs within the first hour. Fig. 1B shows that the solution composition had a significant impact on the adsorption capacity of TBT by medium PS-NP, this is shown by $C_{aqueous}$ in pH 8 Milli-Q water plateauing at a concentration 82% lower than ASW. To ensure the TBT adsorption in the following isotherm experiments had fully equilibrated, each batch of vials was left for 24 hours.

Thermodynamics of adsorption

Isotherms for PS-NP in Milli-Q water at pH 8. It was found that, in all cases, the Freundlich model (eqn (1)) exhibited adjusted R^2 values closer to 1 and was therefore considered the more appropriate fit.

The pH 8 phosphate buffer (in Milli-Q water) was used to model the adsorption behaviour across a wide range of initial concentrations. The results show the relationship of a Freundlich isotherm, where the exponential fitting displayed the best correlation (Fig. 2A). The exponential relationship can be explained either by precipitation or substantial multi-layer adsorption of TBT.[62,63] Multi-layer adsorption occurs when the sorbed TBT provides additional binding sites for adsorption, allowing more TBT to become sorbed in multiple layers. This multilayer can be formed as a result of physical adsorption mechanisms such as electrostatic interactions or
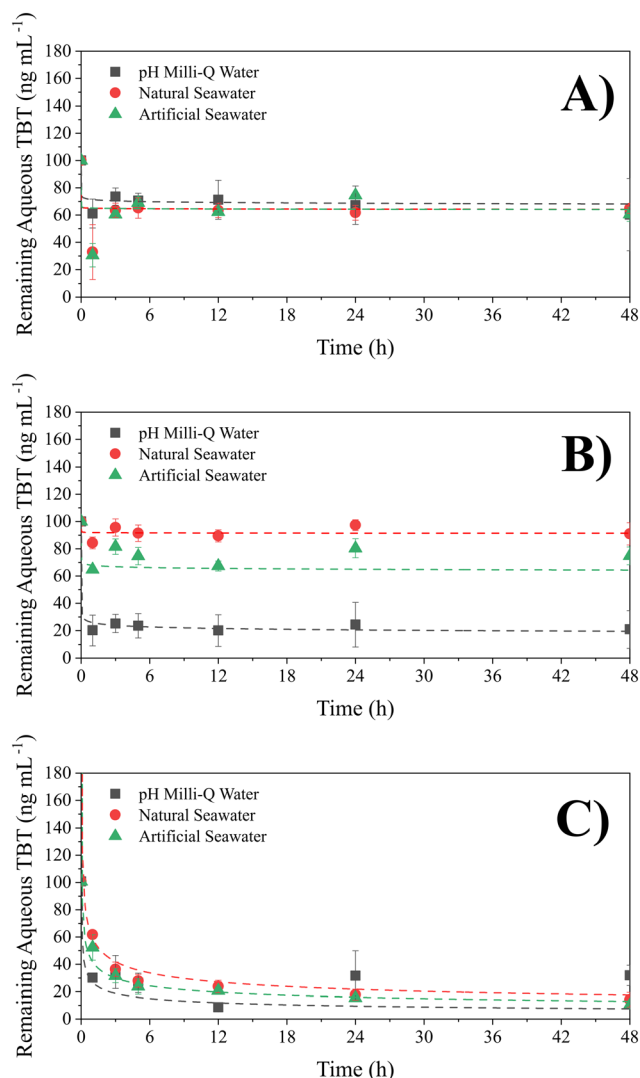
This journal is © The Royal Society of Chemistry 2024

Environ. Sci.: Nano, 2024, **11**, 241–252 | **245**

Fig. 1 Kinetics of TBT adsorption by PS-NP, showing the relationship between aqueous TBT concentration (ng mL^{-1} TBT) and time (h) during kinetics experiments. A) Large PS-NP, B) medium PS-NP and C) small PS-NP. Experimental replicates are represented with error bars (SD, n = 3).
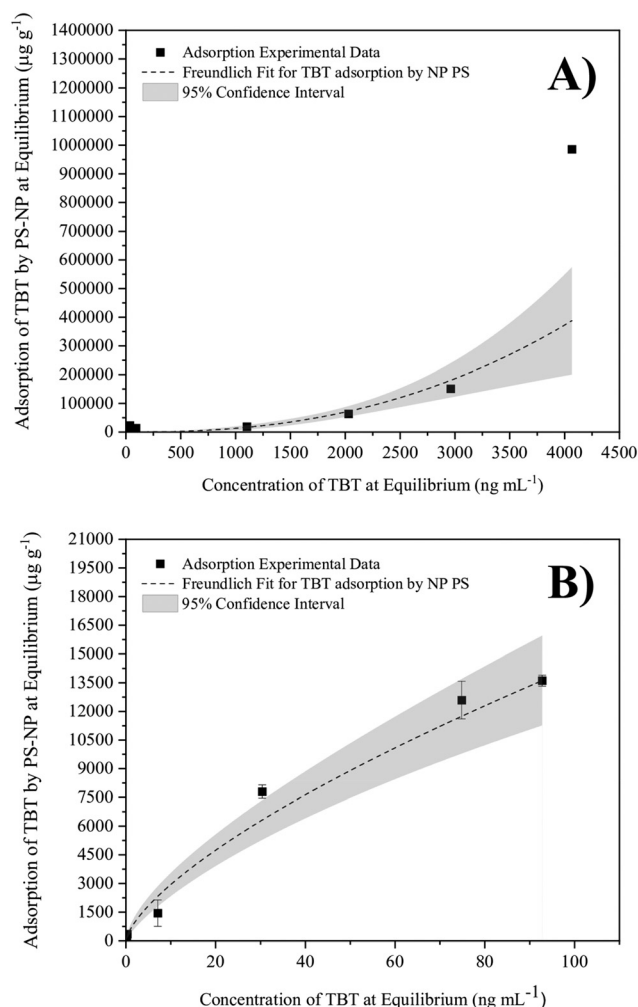

Fig. 2 Adsorption of TBT by large PS-NP in pH 8 Milli-Q water, showing Freundlich fitting for TBT adsorption in phosphate pH 8 Milli-Q buffer across A) an extended concentration range and B) a concentration range limited by the TBT solubility limit.

hydrogen bonding.[64] Precipitation occurs when the hydrophobic TBT has reached its limit of solubility, therefore being removed from the aqueous phase *via* precipitation rather than adsorption. TBT has a relatively low aqueous solubility, ranging from parts per billion (ng mL^{-1}) to parts per million (μg mL^{-1}) levels with examples of 1 to 15 μg mL^{-1} in distilled water[55,65,66] and 300 to 800 ng mL^{-1} TBT in salt water.[46,55,65] In this research, the aqueous solubility of TBT in ASW was taken to be 300 ng mL^{-1} TBT at room temperature.[55] Thus, when excluding the data points above 300 ng mL^{-1} TBT, the relationship reverts to the standard logarithmic shape of a Freundlich isotherm (Fig. 2B). This shape represents the mono-layer adsorption of TBT onto PS-NP. Therefore, Fig. 2 provides evidence that, at concentrations greater than 300 ng mL^{-1} TBT, the TBT is undergoing precipitation instead of becoming sorbed onto the PS-NP.

Isotherms for PS-NP in artificial and natural seawater. To avoid any precipitation mechanisms, the adsorption was performed across a narrower concentration range (10–200 ng mL^{-1} TBT, Fig. 3). The non-linear Freundlich models are given in Fig. 3A–C and the linearised Freundlich forms are given in Fig. 3D–F. Freundlich parameters for each of the non-linear plots are provided in Table S2 in the ESI.† The values obtained from the isotherm plots can be used to determine the relative adsorption of the PS-NP within each of the water matrices.

Fig. 3A and B show that TBT adsorption by large and medium PS-NP within the ASW and NSW matrices is approaching saturation within the tested range. In both cases, the isotherms begin to show signs of plateauing as they approach 150 ng mL^{-1} TBT. However, adsorption within the water with intermediate salinity, *i.e.* brackish water, does not appear to approach saturation. Instead, the curve remains linear within the tested range, suggesting more favourable adsorption due to the greater 1/n value. This is
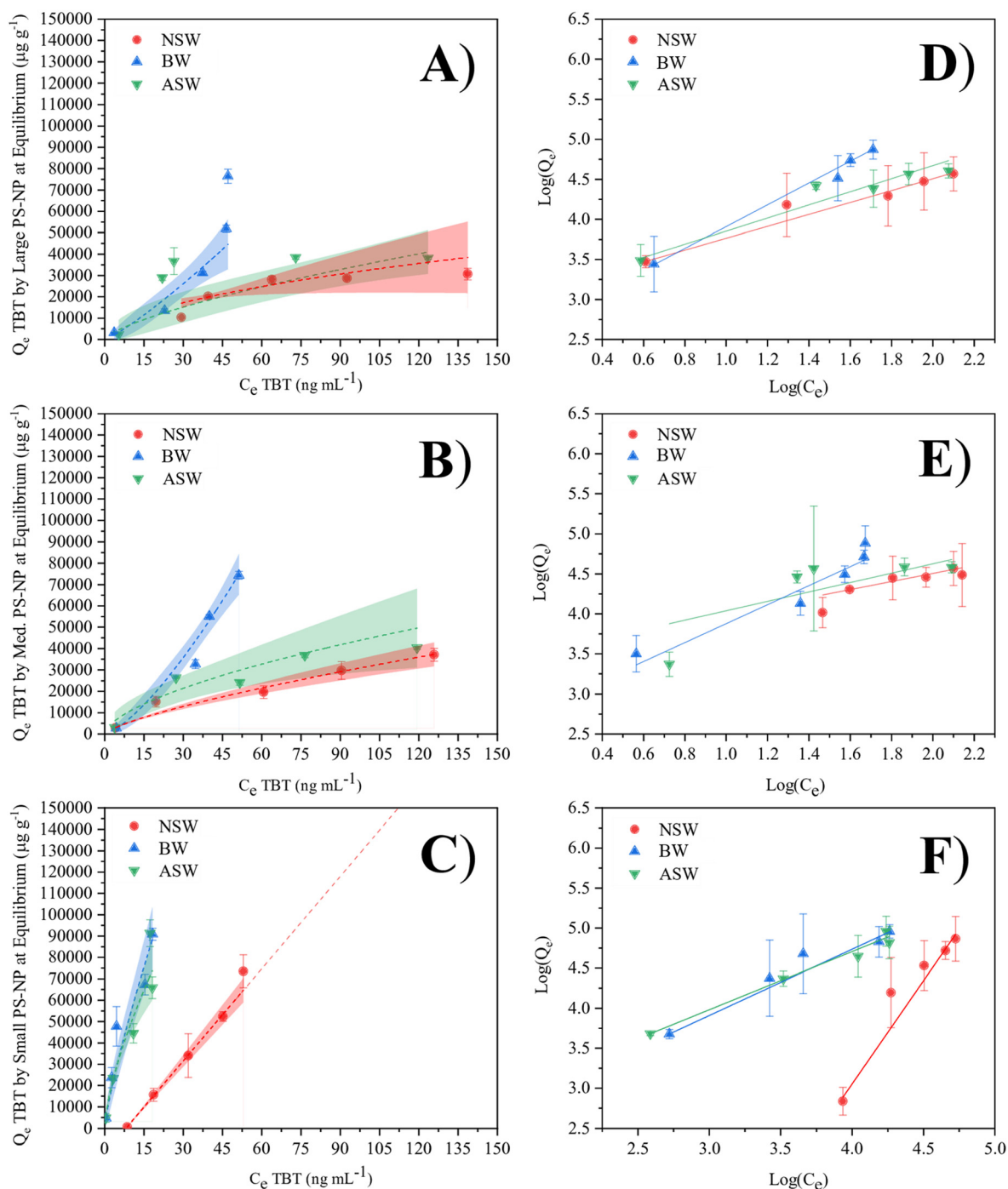
246 | *Environ. Sci.: Nano*, 2024, **11**, 241–252

This journal is © The Royal Society of Chemistry 2024

Fig. 3 Freundlich fitting for TBT adsorption by varying size of polystyrene nanoplastic (large (A), medium (B), small (C)) in natural seawater (red circle), brackish water (blue triangle), and artificial seawater (green inverted triangle) across an environmentally occurring concentration range. Shaded regions display the 95% confidence intervals. Linearised Freundlich models for large (D) medium (E) and small (F) particles.

due to there being less competition with other aqueous salt ions. Because of this, TBT is able to sorb more readily because it has better access to binding locations on the plastic particle. In the cases where the Freundlich isotherms are effectively linear, such as the small PS and brackish water matrices, it can be inferred that the sorption of TBT onto PS-NP is directly proportional to the concentration of TBT within the given concentration range.

Due to the relationship between K_F, Q_{max} and K_A, K_F can be used as an indicator of adsorption capacity, however, it is important to consider that n is also a controlling factor. For example, K_F for each BW isotherm is small; but, due to an n value of less than 1, the adsorption capacity is significantly greater than the K_F constant suggests. As a result of this dependency, the Freundlich isotherm and K_F cannot be used to calculate the maximum adsorption capacity directly. In

This journal is © The Royal Society of Chemistry 2024

Environ. Sci.: Nano, 2024, **11**, 241–252 | **247**

general, the value of n should not be less than 1. In the brackish water, $n < 1$ for both the large and medium particles. This is due to the steepness of the curve at the lower concentrations, and suggests that the maximum adsorption capacity is limited by the aqueous concentration of TBT rather than the sorption potential of PS-NP. The close mirroring in adsorption behaviour between the artificial and natural seawater suggest that artificial seawater can be used as an alternative to natural seawater in future modelling of environmental systems, whilst eliminating the need to account for pollutants of non-interest.

Calculation of adsorption parameters. Freundlich parameters were calculated using the linearised models (Fig. 3C–E). Freundlich parameters were substituted into eqn (3) to obtain the approximated adsorption capacity (Q_{sat}). The calculated parameters (Q_{sat} and K_D) for the 3 sizes of PS-NP and all water matrices are presented in Fig. S11 in the ESI.† The percentage (m/m) of adsorption calculated from Q_{sat} values for 3 sizes of PS-NP and all water matrices are shown in Fig. 4 ($Q_{sat} \propto$ % (m/m)).

The approximated adsorption capacities (Q_{sat}) confirm the current literature hypothesis of NPs having a greater adsorption potential than MPs, with the smallest PS particle size exhibiting large Q_{sat} values for each of the 3 water matrices. This is likely due to the significantly larger surface area of the smallest particles (109 ± 5 m^2 g^{-1} for small PS, when compared to 2.3 ± 0.1 m^2 g^{-1} for medium PS and 1.2 ± 0.1 m^2 g^{-1} for large PS), allowing for an increase in available binding sites for TBT. When normalising the adsorption capacity to the surface area, smaller PS-NP particles are shown to sorb less TBT per m^2 (Table S3, ESI†). However, because the small PS-NP latex contains more particles per unit volume, the total surface area and therefore the total

adsorption capacity is greater. Fig. 4 shows that the PS-NP size has less of an effect on the adsorption capacity in brackish water than seawater, with similar Q_{sat} values for large and small PS-NP in BW. Further work may need to be completed to fully understand the difference in adsorption capacity for the medium size PS particles in BW.

K_D values for TBT adsorption vary significantly in the literature, with reported values for TBT adsorption by sediment particles ranging between 0.1 and 8200 L g^{-1}.[46,47,67–69] This variation is likely caused by a combination of factors; notably, the composition and size of sediment as well as physical conditions such as temperature, pH and salinity. There is a current lack of literature values for the distribution coefficient of TBT by plastic particles – likely due to the analytical challenges associated with NPs. The calculated K_D values from this research lie within the upper range of the reported values for sediment in the literature, suggesting that NPs have similar pollutant sorption potential to naturally occurring particles.

Mechanism of adsorption

To elucidate whether TBT undergoes chemi- and/or physisorption, it is possible to gain some understanding of the extent of each mechanism *via* the characterisation of the PS-NP particles pre- and post-adsorption experiments. If the particles exhibit structural collapse, or changes to their surface chemistry, then chemisorption is likely to have taken place. The changes may be viewed using various visualisation techniques such as SEM/TEM-EDS or surface analysis techniques such as FTIR or Raman. In previous research, changes in surface chemistry by copper adsorption,[70] and organic adsorbates on gold substrates[71] have been observed. If the surface structure of the PS-NP remains unchanged, then this could indicate that the adsorption was exclusively physisorption, or that the technique does not have adequate sensitivity[72] to detect changes in the PS-NP surface caused by chemisorption.

In this research, Raman was used to characterise the PS-NP particles at varying points during the adsorption experiments. Spectra were taken of the monomer, crude polymer, purified polymer, and polymer after exposure to TBT during adsorption experiments. Raman spectra are provided in Fig. S12–S14 in the ESI.† The spectra show that there is no appreciable peak shift between the spectra taken prior and post adsorption. Therefore, it is undetermined whether the adsorption behaviour follows a chemi- or physisorption mechanism due to the sensitivity of the instrument.

It is speculated that the mechanism of TBT adsorption on PS-NP follows a combination of both chemi- and physisorption. The equilibrium between TBT$^+$ and TBTOH[73] allows for electrostatic interactions between negatively charged oxylated groups on the surface of the plastic particle, as well as hydrogen bonding *via* the hydroxy group of TBTOH.[74] In addition, the long, non-polar alkyl chains
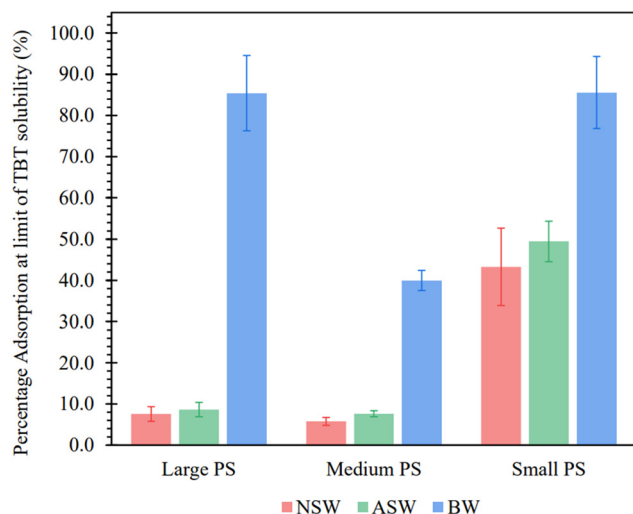

Fig. 4 Adsorption capacity (%) of large, medium and small PS particles in natural seawater (NSW), artificial seawater (ASW) and brackish water (BW). Key statistical differences are shown, comparing NSW, ASW and BW, large with medium PS, medium with small PS and large with small PS. Columns labelled with different letters are significantly different ($p < 0.05$), $N = 4$.

248 | *Environ. Sci.: Nano*, 2024, **11**, 241–252

This journal is © The Royal Society of Chemistry 2024

interact physically with the surface of the organic polymer. It is perhaps due to this combination of sorption mechanisms that TBT can undergo multi-layer adsorption as described by the Freundlich model.

Conclusion

Polystyrene particles were produced in 3 distinct size classes spanning the nanoplastic range. Kinetics and thermodynamics of TBT adsorption by nanopolystyrene were investigated. Kinetic modelling showed that the adsorption was very quick to progress, with the majority of adsorption taking place within the first 3–12 hours (Fig. 1). Thermodynamic experimental data were most closely modelled using the Freundlich isotherm (Fig. 3), suggesting that TBT underwent multi-layer adsorption. Experiments utilising Raman did not provide indication whether chemisorption took place. It was speculated that the binding mechanism was likely a combination of physical and chemical interactions, such as hydrogen bonding, electrostatic attraction, and van der Waals.

Freundlich parameters K_F and n were derived from each isotherm. These parameters can be used as relative indicators of adsorption behaviour, however Freundlich was unable to definitively assign physical significance to them.[46] Alternatively, the adsorption capacity was approximated using the maximum aqueous solubility limit of TBT (taken as 300 ng mL^{-1} TBT). The approximated adsorption capacity Q_{sat} gave an indication of the absolute maximum mass of TBT to be adsorbed onto the surface of the plastic particles, limited by the aqueous concentration of TBT. Q_{sat} was also used to determine the partition coefficient K_D of TBT between the solid and aqueous phases.

Despite its legislative ban, TBT remains persistent in the marine environment, reports of imposex within gastropods are still common,[36] and TBT products are still available in the market.[45] This highlights the importance of continuing to monitor and model TBT behaviour and environmental impacts due to the risk of TBT remobilisation and the underestimation of NPs within the ocean. K_D values calculated in this research aligned with some of the larger reported values in the literature for TBT adsorption by sediment, demonstrating that the pollution of NPs into the ocean has provided another vector for the remobilisation of TBT into the water column. It was found that sorption was greatest on the smallest PS-NP size. The increased mobility of NPs *versus* sediment particles may also suggest that TBT bound to NPs could be more available to marine organisms closer to the surface (*i.e.*, those living in tidal zones) than TBT bound to sediment particles. Therefore, further work should be completed to determine the availability of sorbed TBT to these organisms, so that the hazards NPs pose in combination with TBT are fully understood.

Conflicts of interest

There are no conflicts of interest to declare.

Acknowledgements

References

1 R. Geyer, J. R. Jambeck and K. L. Law, Production, use, and fate of all plastics ever made, *Sci. Adv.*, 2017, **3**(7), e1700782.

2 R. C. Thompson, Y. Olson, R. P. Mitchell, A. Davis, S. J. Rowland and A. W. G. John, *et al.*, Lost at Sea: Where Is All the Plastic?, *Science*, 2004, **304**(5672), 838.

3 E. Van Sebille, C. Wilcox, L. Lebreton, N. Maximenko, B. D. Hardesty and J. A. Van Franeker, *et al.*, A global inventory of small floating plastic debris, *Environ. Res. Lett.*, 2015, **10**(12), 124006.

4 E. Danopoulos, L. C. Jenner, M. Twiddy and J. M. Rotchell, Microplastic Contamination of Seafood Intended for Human Consumption: A Systematic Review and Meta-Analysis, *Environ. Health Perspect.*, 2020, **128**(12), 126002.

5 M. Al-Sid-Cheikh, S. J. Rowland, K. Stevenson, C. Rouleau, T. B. Henry and R. C. Thompson, Uptake, Whole-Body Distribution, and Depuration of Nanoplastics by the Scallop Pecten maximus at Environmentally Realistic Concentrations, *Environ. Sci. Technol.*, 2018, **52**(24), 14480–14486.

6 C. G. Avio, S. Gorbi and F. Regoli, Experimental development of a new protocol for extraction and characterization of microplastics in fish tissues: First observations in commercial species from Adriatic Sea, *Mar. Environ. Res.*, 2015, **111**, 18–26.

7 P. A. Da Costa Filho, D. Andrey, B. Eriksen, R. P. Peixoto, B. M. Carreres and M. E. Ambühl, *et al.*, Detection and characterization of small-sized microplastics (≥ 5 μm) in milk products, *Sci. Rep.*, 2021, **11**(1), 24046.

8 A. Ragusa, V. Notarstefano, A. Svelato, A. Belloni, G. Gioacchini and C. Blondeel, *et al.*, Raman Microspectroscopy Detection and Characterisation of Microplastics in Human Breastmilk, *Polymers*, 2022, **14**(13), 1–13.

9 S. Abbasi, B. Keshavarzi, F. Moore, A. Turner, F. J. Kelly and A. O. Dominguez, *et al.*, Distribution and potential health impacts of microplastics and microrubbers in air and street dusts from Asaluyeh County, Iran, *Environ. Pollut.*, 2019, **244**, 153–164.

10 S. A. Mason, V. G. Welch and J. Neratko, Synthetic Polymer Contamination in Bottled Water, *Front. Chem.*, 2018, **6**, 407.

This journal is © The Royal Society of Chemistry 2024

Environ. Sci.: Nano, 2024, **11**, 241–252 | **249**

11 B. E. Oßmann, G. Sarau, H. Holtmannspötter, M. Pischetsrieder, S. H. Christiansen and W. Dicke, Small-sized microplastics and pigmented particles in bottled mineral water, *Water Res.*, 2018, **141**, 307–316.

12 F. Welle and R. Franz, Microplastic in bottled natural mineral water - literature review and considerations on exposure and risk assessment, *Food Addit. Contam.: Part A*, 2018, **35**(12), 2482–2492.

13 L. M. Hernandez, E. G. Xu, H. C. E. Larsson, R. Tahara, V. B. Maisuria and N. Tufenkji, Plastic Teabags Release Billions of Microparticles and Nanoparticles into Tea, *Environ. Sci. Technol.*, 2019, **53**(21), 12300–12310.

14 J. Li, D. Yang, L. Li, K. Jabeen and H. Shi, Microplastics in commercial bivalves from China, *Environ. Pollut.*, 2015, **207**, 190–195.

15 J. Gigault, B. Pedrono, B. Maxit and A. Ter Halle, Marine plastic litter: The unanalyzed nano-fraction, *Environ. Sci.: Nano*, 2016, **3**(2), 346–350.

16 Science Advice for Policy by European Academies (SAPEA). A scientific perspective on microplastics in nature and society – SAPEA, 2019 Jan.

17 K. Boyle and B. Örmeci, Microplastics and Nanoplastics in the Freshwater and Terrestrial Environment: A Review, *Water*, 2020, **12**(9), 2633.

18 F. Yu, C. Yang, Z. Zhu, X. Bai and J. Ma, Adsorption behavior of organic pollutants and metals on micro/nanoplastics in the aquatic environment, *Sci. Total Environ.*, 2019, **694**, 133643.

19 X. Wei, M. Li, Y. Wang, L. Jin, G. Ma and H. Yu, Developing Predictive Models for Carrying Ability of Micro-Plastics towards Organic Pollutants, *Molecules*, 2019, **24**(9), 1784.

20 A. Bakir, I. A. O'Connor, S. J. Rowland, A. J. Hendriks and R. C. Thompson, Relative importance of microplastics as a pathway for the transfer of hydrophobic organic chemicals to marine life, *Environ. Pollut.*, 2016, **219**, 56–65.

21 T. Hüffer, A. K. Weniger and T. Hofmann, Sorption of organic compounds by aged polystyrene microplastic particles, *Environ. Pollut.*, 2018, **236**, 218–225.

22 F. Wang, M. Zhang, W. Sha, Y. Wang, H. Hao and Y. Dou, *et al.*, Sorption behavior and mechanisms of organic contaminants to nano and microplastics, *Molecules*, 2020, **25**(8), 1827.

23 O. D. Agboola and N. U. Benson, Physisorption and Chemisorption Mechanisms Influencing Micro (Nano) Plastics-Organic Chemical Contaminants Interactions: A Review, *Front. Environ. Sci.*, 2021, **9**, 167.

24 X. Guo, G. Hu, X. Fan and H. Jia, Sorption properties of cadmium on microplastics: The common practice experiment and A two-dimensional correlation spectroscopic study, *Ecotoxicol. Environ. Saf.*, 2020, **190**, 110118.

25 Z. Wang, M. Chen, L. Zhang, K. Wang, X. Yu and Z. Zheng, *et al.*, Sorption behaviors of phenanthrene on the microplastics identified in a mariculture farm in Xiangshan Bay, southeastern China, *Sci. Total Environ.*, 2018, **628–629**, 1617–1626.

26 A. Lee, J. Mondon, A. Merenda, L. F. Dumée and D. L. Callahan, Surface adsorption of metallic species onto microplastics with long-term exposure to the natural marine environment, *Sci. Total Environ.*, 2021, **780**, 146613.

27 T. Wang, L. Wang, Q. Chen, N. Kalogerakis, R. Ji and Y. Ma, Interactions between microplastics and organic pollutants: Effects on toxicity, bioaccumulation, degradation, and transport, *Sci. Total Environ.*, 2020, **748**, 142427.

28 X. Zhang, M. Zheng, X. Yin, L. Wang, Y. Lou and L. Qu, *et al.*, Sorption of 3,6-dibromocarbazole and 1,3,6,8-tetrabromocarbazole by microplastics, *Mar. Pollut. Bull.*, 2019, **138**, 458–463.

29 M. Davranche, C. Veclin, A. C. Pierson-Wickmann, E. Hadri, B. Grassl and L. Rowenczyk, *et al.*, Are nanoplastics able to bind significant amount of metals? The lead example, *Environ. Pollut.*, 2019, 940–948.

30 I. Velzeboer, C. J. A. F. Kwadijk and A. A. Koelmans, Strong sorption of PCBs to nanoplastics, microplastics, carbon nanotubes, and fullerenes, *Environ. Sci. Technol.*, 2014, **48**(9), 4869–4876.

31 B. Dahl and H. Blanck, Pollution-induced community tolerance (PICT) in periphyton communities established under tri-n-butyltin (TBT) stress in marine microcosms, *Aquat. Toxicol.*, 1996, **34**(4), 305–325.

32 E. Oberdörster, J. Romano and P. McClellan-Green, The neuropeptide APGWamide as a penis morphogenic factor (PMF) in gastropod mollusks, *Integr. Comp. Biol.*, 2005, 28–32.

33 B. S. Smith, Sexuality in the American Mud Snail, Nassarius Obsoletus Say, *J. Molluscan Stud.*, 1971, **39**(5), 377–378.

34 B. Antizar-Ladislao, Environmental levels, toxicity and human exposure to tributyltin (TBT)-contaminated marine environment. A review, *Environ. Int.*, 2008, **34**(2), 292–308.

35 E. Zou, Aquatic Invertebrate Endocrine Disruption, in *Encyclopedia of Animal Behavior*, 2nd edn, 2019, vol. 1–5.

36 M. N. Ragagnin and A. Turra, Imposex incidence in the sandy beach snail Hastula cinerea reveals continued and widespread tributyltin contamination after its international ban, *Reg. Stud. Mar. Sci.*, 2022, **49**, 102118.

37 R. G. Uc-Peraza, V. H. Delgado-Blas, J. Rendón-von Osten, Í. B. Castro, M. C. Proietti and G. Fillmann, Mexican paradise under threat: The impact of antifouling biocides along the Yucatán Peninsula, *J. Hazard. Mater.*, 2022, **427**, 128162.

38 S. H. Lee, Y. S. Chen, C. F. Chen, F. P. J. B. Albarico, Y. C. Lim and M. H. Wang, *et al.*, Butyltin Contamination in Fishing Port Sediments after the Ban of Tributyltin Antifouling Paint: A Case of Qianzhen Fishing Port in Taiwan, *Water*, 2022, **14**(5), 813.

39 G. W. Bryan, P. E. Gibbs, G. R. Burt and L. G. Hummerstone, The effects of tributyltin (TBT) accumulation on adult dog-whelks, Nucella lapillus: long-term field and laboratory experiments, *J. Mar. Biol. Assoc. U. K.*, 1987, **67**(3), 525–544.

40 R. B. Laughlin, W. French and H. E. Guard, Accumulation of bis(tributyltin) oxide by the marine mussel Mytilus edulis, *Environ. Sci. Technol.*, 1986, **20**(9), 884–890.

41 J. M. Ruiz, G. W. Bryan and P. E. Gibbs, Acute and chronic toxicity of tributyltin (TBT) to pediveliger larvae of the

250 | *Environ. Sci.: Nano*, 2024, **11**, 241–252

This journal is © The Royal Society of Chemistry 2024

bivalve Scrobicularia plana, *Mar. Biol.*, 1995, **124**(1), 119–126.

42 N. Spooner, P. E. Gibbs, G. W. Bryan and L. J. Goad, The effect of tributyltin upon steroid titres in the female dogwhelk, Nucella lapillus, and the development of imposex, *Mar. Environ. Res.*, 1991, **32**(1–4), 37–49.

43 H. Roach, B. King, K. King and S. Oelrich, The Effects of Tributyltin on the Marine Environment, 2004.

44 I. K. Konstantinou and T. A. Albanis, Worldwide occurrence and effects of antifouling paint booster biocides in the aquatic environment: A review, *Environ. Int.*, 2004, **30**, 235–248.

45 R. G. Uc-Peraza, Í. B. Castro and G. Fillmann, An absurd scenario in 2021: Banned TBT-based antifouling products still available on the market, *Sci. Total Environ.*, 2022, **805**, 150377.

46 N. D. Pope, The Bioavailability of Sediment Bound Tributyltin (TBT), *PhD thesis*, University of Plymouth, 1998, p. 258.

47 W. J. Langston and N. D. Pope, Determinants of TBT adsorption and desorption in estuarine sediments, *Mar. Pollut. Bull.*, 1995, **31**(1–3), 32–43.

48 R. J. Carter, N. J. Turoczy and A. M. Bond, Container Adsorption of Tributyltin (TBT) Compounds: Implications for Environmental Analysis, *Environ. Sci. Technol.*, 1989, **23**(5), 615–617.

49 K. Duis and A. Coors, Microplastics in the aquatic and terrestrial environment: sources (with a specific focus on personal care products), fate and effects, *Environ. Sci. Eur.*, 2016, **28**(1), 1–25.

50 M. Al-Sid-Cheikh, S. J. Rowland, R. Kaegi, T. B. Henry, M. A. Cormier and R. C. Thompson, Synthesis of 14C-labelled polystyrene nanoplastics for environmental studies, *Commun. Mater.*, 2020, **1**(1), 1–8.

51 F. D. L. Leusch and S. Ziajahromi, Converting mg/L to Particles/L: Reconciling the Occurrence and Toxicity Literature on Microplastics, *Environ. Sci. Technol.*, 2021, **55**, 11470–11472.

52 M. Barsbay, O. Güven, M. H. Stenzel, T. P. Davis, C. Barner-Kowollik and L. Barner, Verification of controlled grafting of styrene from cellulose via radiation-induced RAFT polymerization, *Macromolecules*, 2007, **40**(20), 7140–7147.

53 L. Q. Jiang, B. R. Carter, R. A. Feely, S. K. Lauvset and A. Olsen, Surface ocean pH and buffer capacity: past, present and future, *Sci. Rep.*, 2019, **9**(1), 18624.

54 S. Fletcher and G. Woods, Introduction High Throughput, Direct Analysis of Seawater using the Agilent 7800 ICP-MS with HMI for Aerosol Dilution Authors Environmental, 2017.

55 K. Inaba, H. Shiraishi and Y. Soma, Effects of salinity, pH and temperature on aqueous solubility of four organotin compounds, *Water Res.*, 1995, **29**(5), 1415–1417.

56 M. Ben Yahia, Y. Ben Torkia, S. Knani, M. A. Hachicha, M. Khalfaoui and A. Ben Lamine, Models for type VI adsorption isotherms from a statistical mechanical formulation, *Adsorpt. Sci. Technol.*, 2013, **31**(4), 341–357.

57 F. Ambroz, T. J. Macdonald, V. Martis and I. P. Parkin, Evaluation of the BET theory for the characterization of meso and microporous MOFs, *Small Methods*, 2018, **2**, 1800173.

58 S. E. Hachani, A. Meghezzi, M. Slimani and N. Nebbache, Influence of talc incorporation on the thermal properties of polystyrene composites, *Int. J. Chem. Sci.*, 2016, **14**(3), 1236–1242.

59 L. Ding, J. Zhao, Y. Pan, J. Guan, J. Jiang and Q. Wang, Insights into Pyrolysis of Nano-Polystyrene Particles: Thermochemical Behaviors and Kinetics Analysis, *J. Therm. Sci.*, 2019, **28**(4), 763–771.

60 R. El-kharrag, A. Amin and Y. E. Greish, Synthesis and characterization of mesoporous sodium dodecyl sulfate-coated magnetite nanoparticles, *J. Ceram. Sci. Technol.*, 2011, **2**(4), 203–210.

61 D. Ramimoghadam, M. Z. Hussein Bin and Y. H. Taufiq-Yap, The effect of sodium dodecyl sulfate (SDS) and cetyltrimethylammonium bromide (CTAB) on the properties of ZnO synthesized by hydrothermal method, *Int. J. Mol. Sci.*, 2012, **13**(10), 13275–13293.

62 M. Ishiguro, T. Makino and Y. Hattori, Sulfate adsorption and surface precipitation on a volcanic ash soil (allophanic andisol), *J. Colloid Interface Sci.*, 2006, **300**(2), 504–510.

63 G. Németh, L. Mlinárik and Á. Török, Adsorption and chemical precipitation of lead and zinc from contaminated solutions in porous rocks: Possible application in environmental protection, *J. Afr. Earth Sci.*, 2016, **122**, 98–106.

64 N. Sandhyarani, Surface modification methods for electrochemical biosensors, in *Electrochemical Biosensors*, Elsevier, 2019, pp. 45–75.

65 G. Mailhot, M. Astruc and M. Bolte, Degradation of tributyltin chloride in water photoinduced by iron(III), *Appl. Organomet. Chem.*, 1999, **13**(1), 53–61.

66 L. R. Sherman, M. R. Yazdi, H. Hoang and J. Talbot, Solubility and the Degradation of Tri-n-Butyltin Compounds in Aqueous Media, *Proc. Pa. Acad. Sci.*, 1985, **59**(2), 162–166.

67 J. R. W. Harris, I. I. Clearyl and A. D. Valkirs, Particle-Water Partitioning and the Role of Sediments as a Sink and Secondary Source of TBT, in *Organotin*, 1996, pp. 459–473.

68 L. Randall and J. H. Weber, Adsorptive behavior of butyltin compounds under simulated estuarine conditions, *Sci. Total Environ.*, 1986, **57**, 191–203.

69 M. A. Unger, G. Macintyre, R. J. Huggett and M. Creek, *Equilibrium Sorption of Tributyltin Chloride by Chesapeake Bay Sediments Michae*, IEEE, 1987, CH249 & 4/87.

70 C. Mongiovi, G. Crini, X. Gabrion, V. Placet, V. Blondeau-Patissier and A. Krystianiak, *et al.*, Revealing the adsorption mechanism of copper on hemp-based materials through EDX, nano-CT, XPS, FTIR, Raman, and XANES characterization techniques, *Chem. Eng. J. Adv.*, 2022, **10**(12), 100282.

71 Z. F. Cai, N. Kumar and R. Zenobi, Probing On-Surface Chemistry at the Nanoscale Using Tip-Enhanced Raman Spectroscopy, *CCS Chem.*, 2023, **5**, 55–71.

72 A. Otto, I. Mrozek, H. Grabhorn and W. Akemann, *et al.*, Surface-enhanced Raman scattering, *J. Phys.: Condens. Matter*, 1992, **4**, 1143–1212.

This journal is © The Royal Society of Chemistry 2024

Environ. Sci.: Nano, 2024, **11**, 241–252 | **251**

73 R. B. Laughlin, H. E. Guard and W. M. Coleman, Tributyltin in Seawater: Speciation and Octanol-Water Partition Coefficient, *Environ. Sci. Technol.*, 1986, **20**(2), 201–204.

74 F. Wang, M. Zhang, W. Sha, Y. Wang, H. Hao and Y. Dou, *et al.*, Sorption behavior and mechanisms of organic contaminants to nano and microplastics, *Molecules*, 2020, **25**(8), 1827.